Biomedical Signal Processing and Control 8 (2013) 30–40

Contents lists available at SciVerse ScienceDirect

Biomedical Signal Processing and Control

journal homepage: www.elsevier.com/locate/bspc

FISH image analysis using a modified radial basis function network

Christos Sagonas [a], Ioannis Marras [a,*], Ioannis Kasampalidis [a], Ioannis Pitas [a], Kleoniki Lyroudia [b], Georgia Karayannopoulou [c]

[a] Aristotle University of Thessaloniki, Department of Informatics, Box 451, 54124 Thessaloniki, Greece
[b] Aristotle University of Thessaloniki, Department of Endodontology, Dental School, 54124 Thessaloniki, Greece
[c] Aristotle University of Thessaloniki, Department of Pathology, Medical School, 54124 Thessaloniki, Greece

ARTICLE INFO

Article history:
Received 22 October 2011
Received in revised form 26 April 2012
Accepted 14 May 2012
Available online 2 June 2012

Keywords:
FISH
Cell nucleus segmentation
Spot detection
HER-2/neu
Gene amplification

ABSTRACT

Fluorescent in situ hybridization (FISH) is an exceptionally useful method in determining HER-2/neu gene status in breast carcinoma samples, which is a valuable cancer prognostic indicator. Its visual evaluation is a difficult task, which involves manual counting of red/green dots in multiple microscopy images, a procedure which is both time consuming and prone to human errors. A number of algorithms have recently been developed dealing with the (semi)-automated analysis of FISH images. Their performance is quite promising, but further improvement is required in their diagnostic accuracy. In addition, they have to be evaluated on large FISH image data sets. Here, we present a novel method for analyzing FISH images based on cell nuclei and red/green spot modelling by radial basis functions (RBFs). Our method was compared to one of the most prominent methods reported in the literature on a large data set, comprised of 246 breast cancer cases (in total 3412 FISH images) and showed statistically significant diagnostic accuracy improvement, especially on HER-2/neu positive cases. The overall diagnostic accuracy of the proposed method is 95.93% over this data set.

© 2012 Elsevier Ltd. All rights reserved.

1. Introduction

Fluorescence in situ hybridization is an established diagnostic method for gene status evaluation. It is essential in determining the status of HER-2/neu gene in breast samples, a valuable cancer prognostic and diagnostic indicator [1]. The HER-2/neu (c-erbB2) oncogene encodes the production of the HER-2/neu receptor, which is a tyrosine kinase receptor that is over-expressed in approximately 20–30% of high-grade invasive breast carcinomas. Since HER-2 positive tumors can be more aggressive, knowing that a cancer is HER-2/neu positive helps in selecting the appropriate treatment. Overexpression of the protein product of HER-2/neu gene is usually a consequence of gene amplification, in which multiple copies of the gene appear throughout the genome. Thus, it is possible to determine the HER-2/neu status, either by analyzing the numbers of gene copies in the nucleus or the amount of the related protein on the cell membrane. Fluorescence in situ hybridization (FISH) is a widely used technology to determine HER-2/neu status that allows a gene copy count. A typical FISH image of HER-2/neu is shown in Fig. 1(a). The cell nuclei have blue color, while the green and red spots map the CEP 17 and the HER-2/neu genes, respectively. The ratio of the red/green spot numbers determines the HER-2/neu status (replication) in each cell nucleus. Alternatively, the amount of protein expression can be measured directly via immunohistochemistry (IHC). There are trade-offs in choosing one of these techniques. Both techniques permit the study of small amounts of formalin-fixed, paraffin-embedded tissue and the interpretation of the findings on a cell-by-cell basis. FISH allows selective staining of various DNA sequences with fluorescent markers and, thereby, the detection, analysis and quantification of specific numerical and structural DNA abnormalities within the nuclei. It is a direct in situ technique that is relatively rapid and sensitive. No cell culture is needed in order to apply this method and results are easier to interpret than karyotype. FISH offers a more objective scoring system, based on the presence of the two HER-2 gene signals (red/green spots) present in all cells of the specimen. Its disadvantages include the high cost of each test, the long time needed for slide scoring, the use of a fluorescence microscope, the inability to preserve the acquired sample for long storage and review, and, occasionally the difficulty in identifying the invasive tumor cells [2]. In [3,4], it has been shown that this procedure is as accurate as Southern blot analysis, while allowing the measurement of the fraction of amplified cells and the intercellular heterogeneity within a given tumor cell population. On the other hand, the advantages of IHC testing include its wide availability, relatively low cost, easy and long preservation of stained slides, while the use of specific antibodies to stain proteins in situ allows the identification of several cell types that could be

* Corresponding author. Tel.: +30 2310996361; fax: +30 2310998453.
E-mail address: imarras@aiia.csd.auth.gr (I. Marras).

1746-8094/$ – see front matter © 2012 Elsevier Ltd. All rights reserved.
http://dx.doi.org/10.1016/j.bspc.2012.05.001

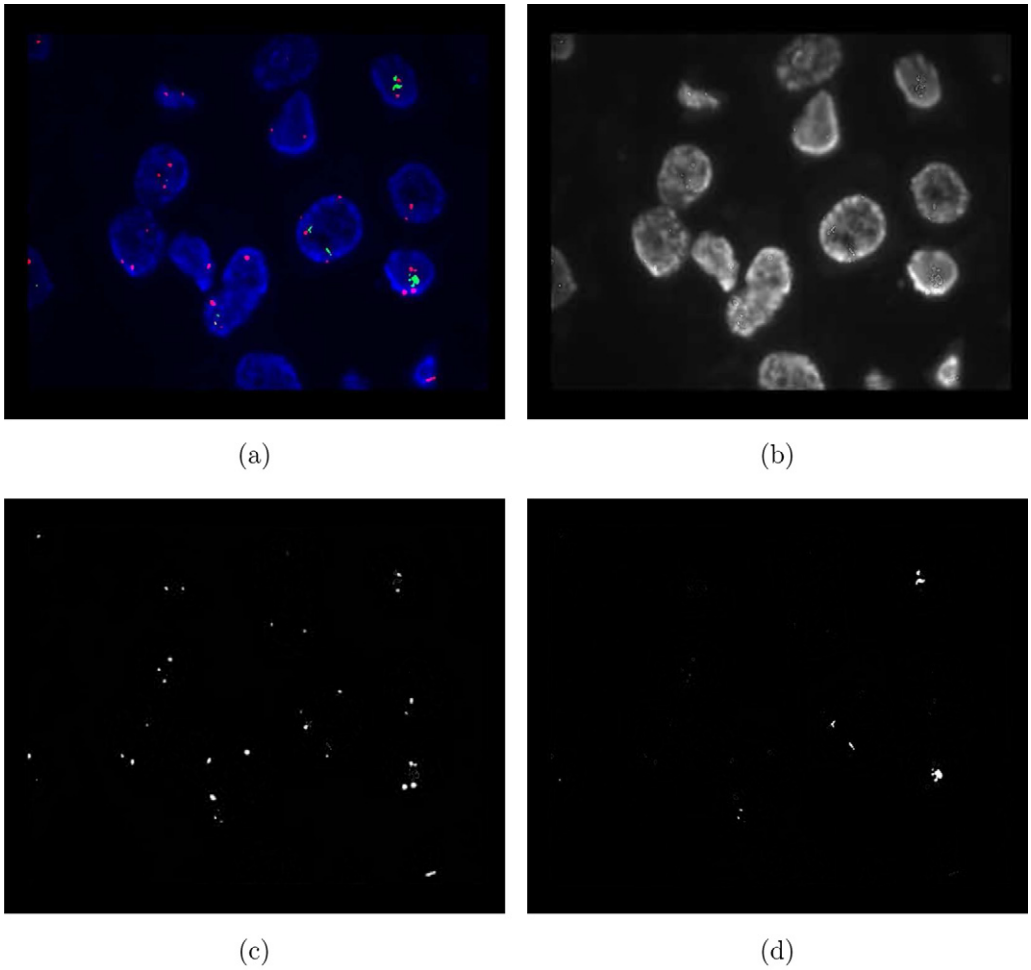

Fig. 1. (a) FISH image, (b) blue channel depicting all nuclei, (c) red channel spots depicting HER-2/neu gene positions, and (d) green channel dots depicting CEP 17 positions. (For interpretation of the references to color in this figure legend, the reader is referred to the web version of the article.)

visualized by classical microscopy. The disadvantages of IHC include the impact of pre-analytic issues, including storage, duration and nature of system control samples and, most importantly, the difficulties in applying a subjective slide scoring system [2]. More specifically, in IHC testing, the reader must judge the degree of color change in the nucleus, against a non-standardized chart. A recent study [5] considered the accuracy, reproducibility and availability of different techniques for the evaluation of HER-2/neu status and recommended patient screening by immunohistochemistry, followed by FISH testing in cases with intermediate staining intensity (cases scored 2^+ according to HercepTest). They suggested that the use of automated analysis may increase testing precision and predicted a wider future use of FISH analysis, as a more cost-effective technique.

Analyzing FISH images is a difficult task, since manual dot scoring over a large number of nuclei and over different tissue samples is a time consuming and fatiguing operation. Moreover, it is user-dependent in a clinical setting, since different doctors may count dots in slightly different ways, especially in ambiguities, e.g., in the case of dotted red spots or blurred spots. In case there are images containing regions with blurred spots, the pathologists assign to those regions a empirical chosen number of spots. In practice, current analysis of FISH signals is performed in a semi-automated way with the aid of image processing software, which can display the different color channels of a FISH image, as shown in Fig. 1 and apply thresholds for nuclei segmentation. One study [6] has shown strong correlation of the detection results using visual-only and semi-automated methods for evaluating the status of HER-2/neu in breast carcinomas samples. However, dot counting in a semi-automatic manner still remains an impractical procedure for a pathologist, since it requires user intervention for excluding poorly segmented, overlapping, clustered or non-relevant cells [6].

Recently, many of techniques have been proposed for analyzing FISH images targeted to a variety of genes. Most of these consist of a two-step process, namely, nuclei segmentation and spot detection. Notable examples are presented in [7], where histogram-based segmentation was performed for counting FISH signals, and in [8,9], where nuclei segmentation was performed via the ISODATA algorithm [10] and the top-hat transform was used for spot detection, followed by thresholding. In [11], nuclei segmentation was accomplished based on the ISODATA algorithm followed by the distance transform, while spot detection was based on the top-hat transform, followed by the recursive reconstruction algorithm [12]. In [13], segmentation was carried out via bi-level histogram analysis and morphological operations [14], while spot detection was performed using a watershed-like technique, called gradual thresholding. In [15,16], nuclei segmentation was performed on the blue channel, using heuristically derived thresholds and morphological operations, while spot detection was evaluated for a number of different techniques, varying from Bayesian classifiers to neural networks. In [17], nuclei segmentation was based on a variation of the watershed transform, dubbed “gradient-weighted distance transform”. In [18], cell nuclei were segmented nuclei via the watershed transform, while spot detection was performed using three

different techniques, ranging from intensity- to histogram- and watershed transform-based methods. In [19], a minimum cluster distance classifier was used to classify the slides into HER-2 categories, employing IHC microscopy images. In [20], a combined method based on the mathematical morphology, using top-hat and bottom-hat filters and inverse multifractal analysis is suggested for detecting and counting fluorescent dots in FISH images. In [21], the proposed multistage algorithm for the automated classification of FISH images from breast carcinomas is the state of the art method in terms of diagnostic accuracy. The algorithm consists mainly of two stages for nuclei and dot detection. The dot segmentation is performed in the RGB color space and consists of a top-hat filter preprocessing stage followed by grey level template matching to separate real signals from noise. The template matching includes a 2D correlation similarity measure with a suitable spot mask, which is derived from a small number of training spots. Nuclei segmentation is performed on the blue channel (DAPI) image. After a non-linearity correction step, global thresholding [22] is used to identify candidate regions. A geometric rule is applied to distinguish between holes within a nucleus and holes between different nuclei. Finally, the marked watershed transform is used to segment cell nuclei. Combining the two stages allows the measurement of a FISH signal ratio per cell nucleus and consequently, the collective classification of cases, in a manner similar to the clinician's evaluation.

Although the results of FISH image analysis are quite satisfactory, further improvement is desirable, especially regarding nuclei segmentation for overlapping or out-of-focus nuclei and correct spot detection, in cases with excessive debris staining or high gene copy number. Therefore, we hereby present a novel algorithm for FISH image analysis, which provides further improvements to the state of the art. The main advantages of the proposed method is its simplicity and firm foundation on shape modelling using radial basis functions (RBFs). RBFs are good candidates for cell nuclei segmentation, since they can model well ellipsoidal objects, as is the case of both cell nuclei and red/green spots. The proposed method is compared to the one in [21], with results showing significant overall diagnostic accuracy improvement, especially on correctly classifying positive HER-2/neu cases.

This study presents a large-scale evaluation of the proposed method on a data set comprising 246 breast cancer cases provided by the cooperating medical team. Such a study is very important, since the current status of most previous methods is at a point, where large clinical studies are required in order to validate their effectiveness. This is especially critical, because most of the methods reviewed here report some deviations from the ground truth, as determined by the medical experts. The advantages of these trials are twofold, providing further hindsight for algorithm improvement, as well as bringing in the medical experts as active participants of the development process. Furthermore, we have performed a large-scale evaluation and comparison of our method with that described in [21] on the 246 breast cancer cases.

2. Materials

Formalin fixed-paraffin embedded tissue blocks from 246 cases were retrieved from the archives of the Pathology Department of the Medical School, Aristotle University of Thessaloniki, Greece. In total, 3412 FISH images were used in our experiments. The majority of the cases had been submitted to this Department for the Quantification of the Amplification of the HER-2/neu Gene via the FISH Method. Hematoxylin–eosin stained slides were reviewed, before the performance of FISH and were tested by immunohistochemistry for the expression of HER-2 protein, using the commercial test (HercepTest(r), DakoCytomation). Paraffin-embedded tumor sections of 3 μm were stained using the Labeled Streptavidin Avidin Biotin (LSAB) method, following the manufacturer recommendations. The process of evaluating the HER-2/neu status from FISH images involves the manual counting of signals in interphase nuclei, which become visible as colored dots. The FDA approved PathVision Her2 FISH kit (Vysis, Downers Grove, USA) uses DNA probes, which are small segments of actual DNA material. When applied to a tumor tissue sample, the DNA probes target the HER-2/neu gene and attach themselves to their target sequence. This process is called hybridization. The probes carry special fluorescent markers that emit light, when the probes bind to the HER-2 genes. The HER-2 probes are visible as orange stained spots under a fluorescent microscope. We name them red spots through out this paper, since they are best visualized in the red FISH image channel. Similarly, probes for centromere 17 (CEP 17), the chromosome on which the gene HER-2/neu is located, are visible as green spots. The sections are counterstained with DAPI, providing a blue background for the cell nucleus body. The conventional analysis involves scoring the ratio r of HER-2/neu over CEP 17 dots within each cell nucleus and, then, averaging the scores for a number of almost 60 cells. Several FISH images usually need to be read to reach the desired number of dot-including nuclei. A ratio of $r \geq 2.0$ of HER-2/neu to CEP 17 copy number denotes gene amplification.

2.1. FISH for HER-2/neu gene amplification

The copy number of Her/neu gene locus at 17q11.2–q12 and alpha satellite DNA located at band region 17p11.1–q11.1 (CEP 17) was estimated by FISH in interphase cells on paraffin TMA sections (3.5 μm), directly labeled with the PathVysion™ HER-2 DNA probe (Vysis) according to the manufacturer instructions. Briefly, the sections were de-paraffinized by overnight heating at 60 °C and by two xylene washes for 5 min each time, followed by dehydration in 100% ethanol for 5 min twice. The slides were air dried and immersed in pretreatment solution (NaSCN) at 80 °C for 30 min. Proteolysis of neoplastic cells was performed by immersing the slides in protease solution at 37 °C for 12 min. Denaturation of tissue sections mounted on the slides was performed by a solution of formamide in 70%, pH 7.5, at 72 °C for 5 min. Hybridization was carried out by adding to the tissue sections 10 L of LSI HER-2/CEP 17 DNA probe for overnight incubation at 37 °C in a moist chamber. Next day the slides were washed with post-hybridization buffer (2× SSC and 0.3% NP-40) at 72 °C for 5 min. Hybridization signals were enumerated in a Zeiss microscope (Axioskop 2 plus HBO 100) equipped with a high quality ×100 oil immersion objective, an appropriate filters set (EX BP360/51 for DAPI, EX BP485/17 for FITC/spectrum green, EX BP560/18 for rhodamine/spectrum orange) and a computerized imaging system. Sixty nuclei were selected randomly and scored for each tumor specimen. HER-2/neu probe is labeled in spectrum orange and the CEP 17 probe in spectrum green. The FISH images were captured with a computer-controlled digital camera and were pre-processed with the FISH Imager (METASYSTEMS) image processing/acquisition software. An example of a typical FISH image is shown in Fig. 1(a). Its blue, red and green channels are shown in Fig. 1(b–d), respectively, where the cell nuclei, red spots and green spots are easily discernible.

3. Proposed method

FISH image analysis comprises two major tasks, namely nuclei segmentation and spot detection. Here, we describe a novel radial basis function (RBF) approach for both these steps. The structure of overall approach is visualized in Fig. 2.

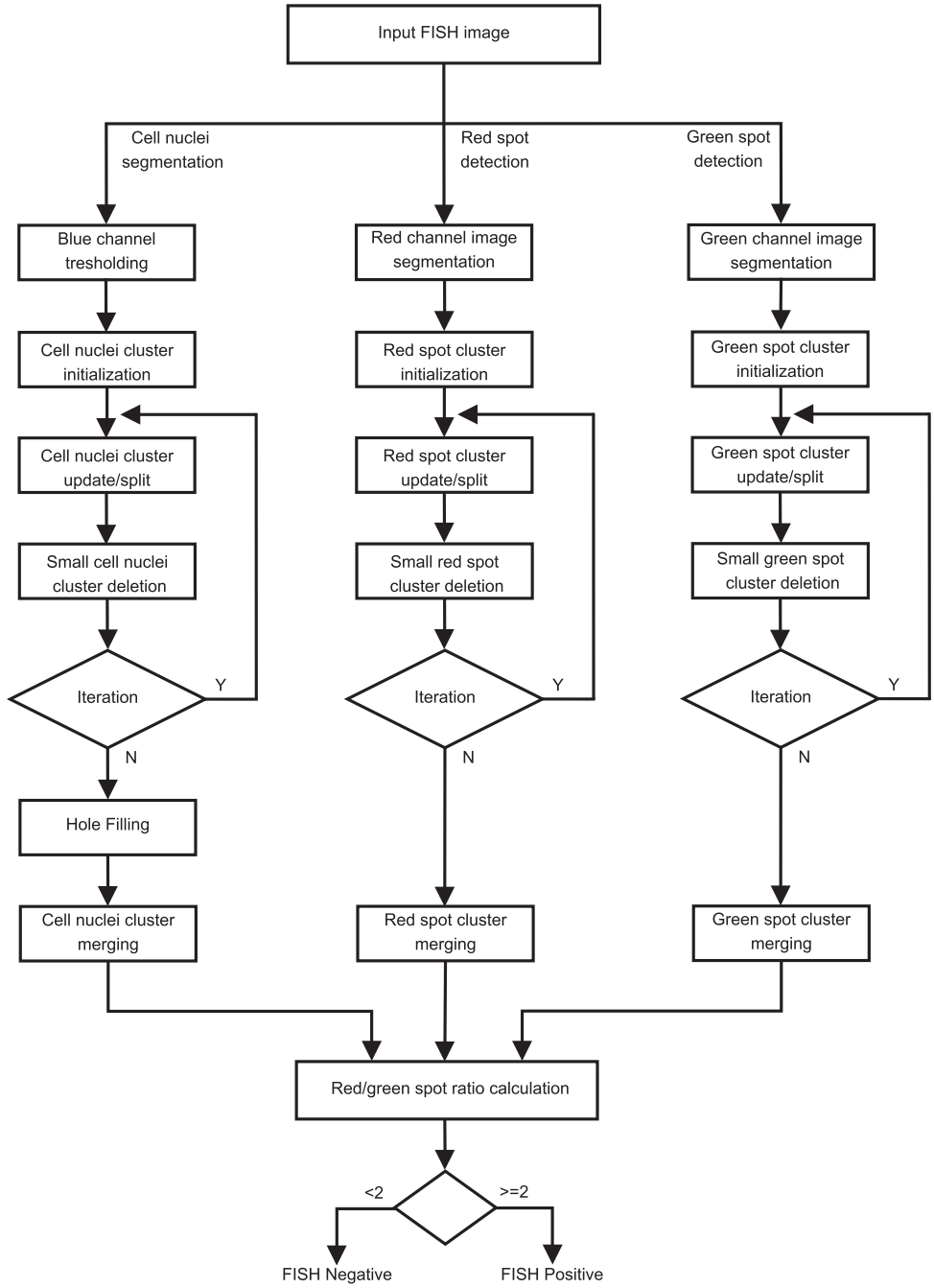

Fig. 2. Flow chart of proposed method for FISH image analysis.

3.1. Nuclei segmentation

Initially, the blue channel is extracted from the original RGB image and the image is subjected to adaptive histogram equalization with default input parameters, as implemented in Matlab®. Next, the image is thresholded and morphological opening/closing is applied with disk-shaped structural elements [23]. In order for the method to perform faster, without affecting its final diagnostic accuracy in a negative way, the last pre-processing step includes image sub-sampling by a suitably chosen factor along both x and y image dimensions that results in images of 150×150 pixels in order to reduce the computational load of subsequent steps.

For nuclei segmentation, a large constant number N of initial nuclei cluster centers $C_{j,j=1,\ldots,N}$ are positioned at uniform x, y intervals throughout the image, while the covariance matrix $\boldsymbol{\Sigma_j}$ of each cluster C_j is initialized to 0. A cluster corresponds to a hidden unit in our RBF network [24]. Ideally, one cluster should correspond to and model one cell nucleus (colored in blue). In general, each hidden unit implements a Gaussian function:

$$\phi_j(\boldsymbol{X}) = \exp[-(\boldsymbol{\mu_j} - \boldsymbol{X})^T \boldsymbol{\Sigma_j}^{-1}(\boldsymbol{\mu_j} - \boldsymbol{X})], \quad j = 1, \ldots, N, \tag{1}$$

where $\boldsymbol{\mu_j}$ is the mean vector and $\boldsymbol{\Sigma_j}$ is the covariance matrix. Geometrically, $\boldsymbol{\mu_j}$ represents the center and $\boldsymbol{\Sigma_j}$ the shape of the jth basis function. A hidden unit function can be represented as a ellipsoid in the 2-dimensional space. A reasonable number of cell nuclei in FISH images of breast cancer is $N = 100$, according to medical experts. This initial number of cluster centers is deemed to be large enough

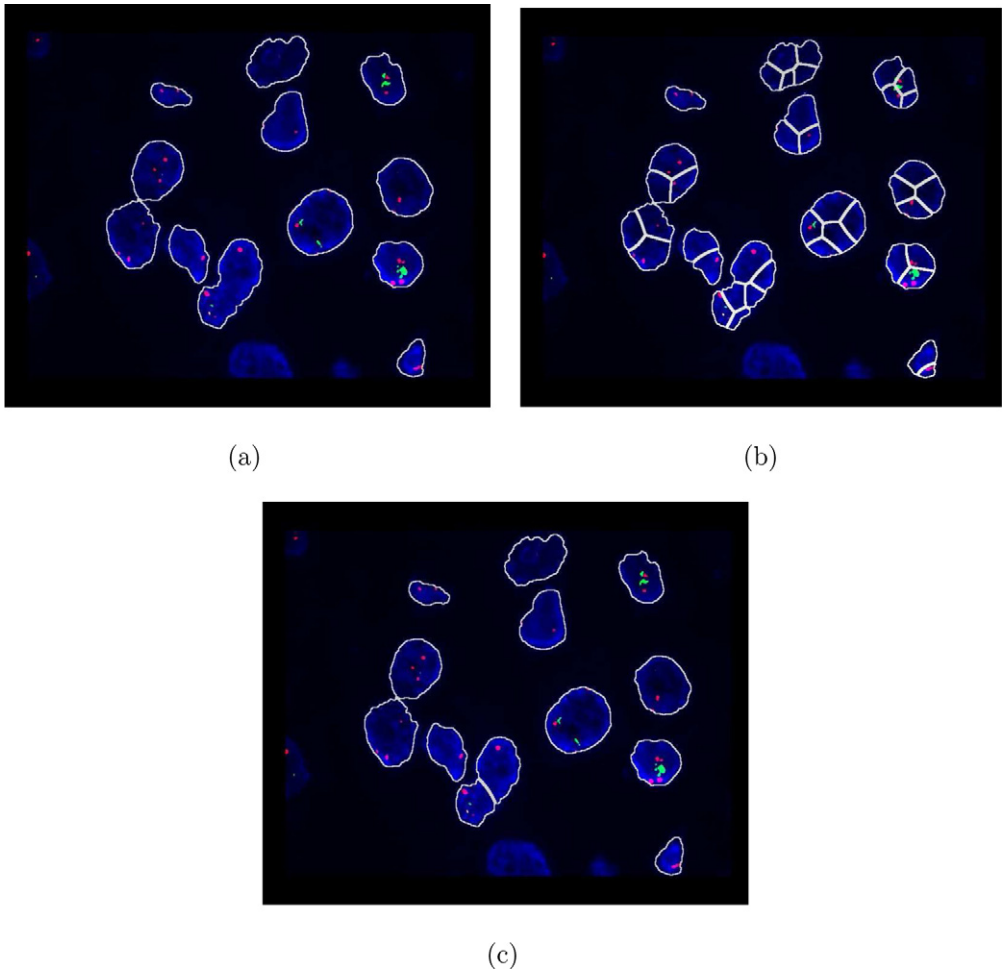

Fig. 3. FISH image segmentation: (a) effect of skipping cluster splitting, (b) effect of skipping cluster merging, and (c) final result of the overall split-merge nuclei segmentation.

to cover the vast majority of the encountered cases. An iterative method is followed for all nuclei segmentation.

In the classical statistics approach, the estimation of the mean and of the covariance matrix for a given population of data samples is given respectively by:

$$E_C[\boldsymbol{\mu_j}] = \frac{\sum_{i=1}^{n_j} \boldsymbol{X_i}}{n_j}, \tag{2}$$

$$E_C[\hat{\boldsymbol{\Sigma}}_{\boldsymbol{j}}] = \frac{\sum_{i=1}^{n_j} (\boldsymbol{X_i} - \boldsymbol{\mu_j})^T (\boldsymbol{X_i} - \boldsymbol{\mu_j})}{n_j - 1}, \tag{3}$$

where $\boldsymbol{X_i}$ is the coordinate vector of the introduced pixel and n_j is the number of data samples from the given data population [25].

Pixels of the thresholded sub-sampled image are introduced sequentially to the clustering algorithm and are then assigned to the closest nuclei cluster. In order to assign each introduced pixel to the closest nuclei cluster according to Learning Vector Quantization (LVQ) algorithm [26], the Euclidean distance is computed between this pixel and each cluster center:

$$\text{If } ||\boldsymbol{X_i} - \boldsymbol{\mu_j}||^2 = \min_{k=1}^{N} ||\boldsymbol{X_i} - \boldsymbol{\mu}_k||^2 \quad \text{then} \quad \boldsymbol{X_i} \in C_j \tag{4}$$

where C_j is the winner cluster. The LVQ algorithm is derived from (2), when the patterns are assigned to an activation region according to (4). In the original LVQ algorithm, used for RBF training, only one center vector is updated, at the iteration $t+1$ according to the rule:

$$\boldsymbol{\mu_j}(t+1) = \boldsymbol{\mu_j}(t) + \eta_j[\boldsymbol{X_i} - \boldsymbol{\mu_j}(t)], \tag{5}$$

where η_j is the learning rate and $\boldsymbol{\mu_j}(t)$ is the nuclei cluster center vector estimated at the iteration t. Various decaying rules for the learning rate were tested for the LVQ algorithm [27]. The learning rate, which achieves the minimum output variance [28], is updated according to [26]:

$$\eta_j = \frac{1}{n_j}, \tag{6}$$

where n_j is the cardinality of nuclei cluster j. For the covariance matrix calculation we use the extension of the LVQ algorithm for second-order statistics [29,30]:

$$\hat{\boldsymbol{\Sigma}}_{\boldsymbol{j}}(t+1) = \frac{n_j - 2}{n_j - 1} \hat{\boldsymbol{\Sigma}}_{\boldsymbol{j}}(t) + \frac{[\boldsymbol{X_i} - \boldsymbol{\mu_j}]^T [\boldsymbol{X_i} - \boldsymbol{\mu_j}]}{n_j - 1}, \tag{7}$$

where $\hat{\boldsymbol{\Sigma}}_{\boldsymbol{j}}(t)$ is the covariance matrix estimate of nuclei cluster j at iteration t. We can observe that the formulas (5) and (7) are the adaptive versions of (2) and (3).

After each new pixel is introduced, a statistical test for cluster splitting is performed, as described in [26]. More specifically, the

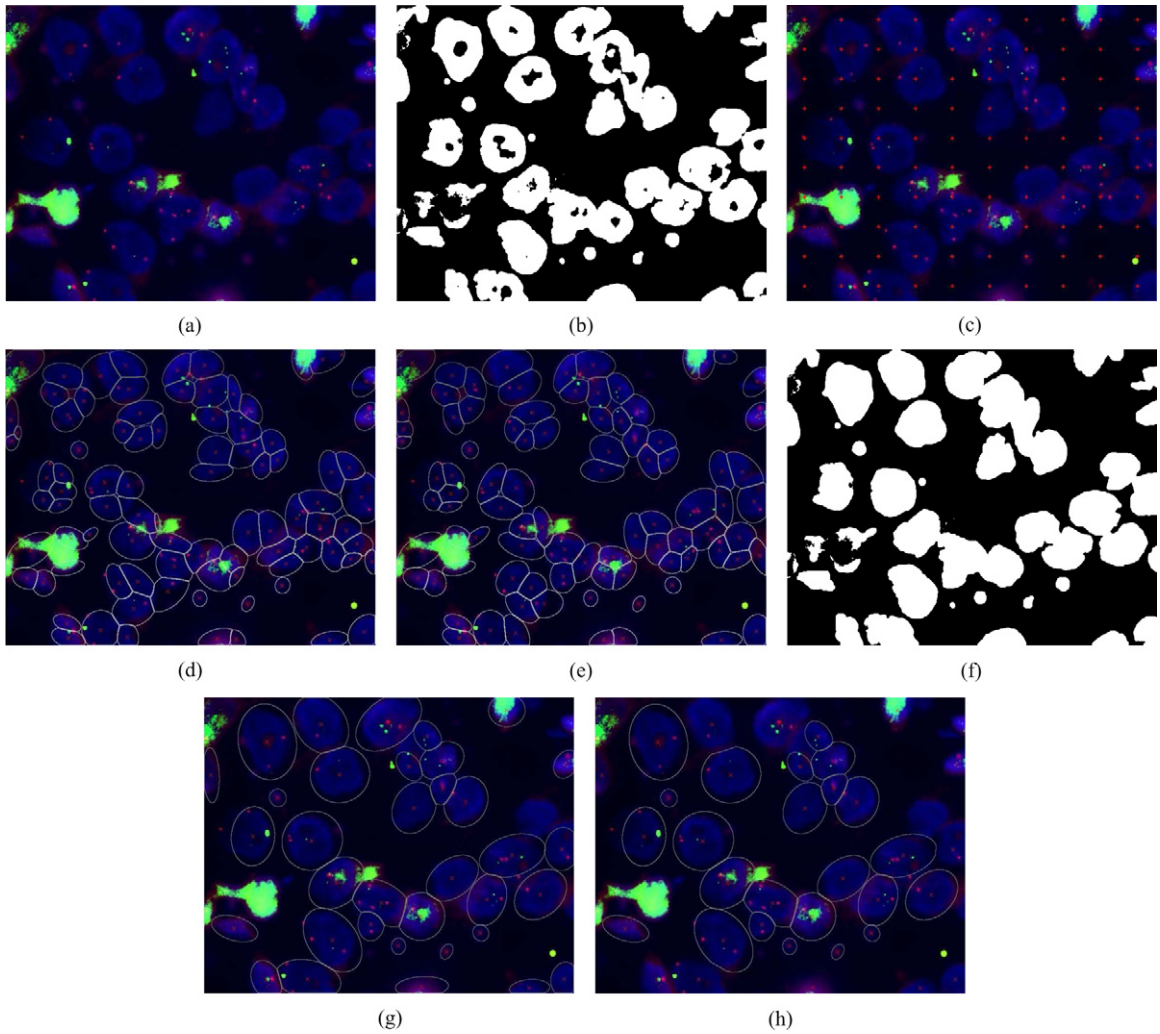

Fig. 4. Intermediate results in cell nuclei segmentation: (a) initial FISH image, (b) blue channel thresholding, (c) cell nuclei cluster initialization (red spots), (d) first iteration of cell nuclei cluster update/split, (e) final result of cell nuclei cluster update/split, (f) hole filing, (g) cell nuclei cluster merging, and (h) deletion of the nuclei that touching image borders. (For interpretation of the references to color in this figure legend, the reader is referred to the web version of the article.)

sum of squared errors of each cluster (measuring cluster dispersion) is defined as:

$$E_j^1 = \sum_{\boldsymbol{X} \in C_j} ||\boldsymbol{X} - \boldsymbol{\mu_j}||^2. \tag{8}$$

If the cluster is split, the sum of squared errors is defined as:

$$E_j^2 = \sum_{\boldsymbol{X} \in C_{j1}} ||\boldsymbol{X} - \boldsymbol{\mu_{j1}}||^2 + \sum_{\boldsymbol{X} \in C_{j2}} ||\boldsymbol{X} - \boldsymbol{\mu_{j2}}||^2, \tag{9}$$

where C_j, C_{j1} and C_{j2} are the original jth cluster and the two clusters resulting from its split, respectively. The split cluster centers are calculated as the center of gravity (arithmetic mean) of the corresponding pixel coordinates. The pixels assigned to each resulting cluster C_{j1}, C_{j2} are found depending on the sign of the following quantity $\underline{\boldsymbol{e}}_j^T(\boldsymbol{X} - \boldsymbol{\mu_j})$ where $\underline{\boldsymbol{e}}_j$ is the principal normalized eigenvector of the cluster C_j. If the previous quantity is positive, the pixel is assigned to cluster C_{j1}, while, if negative, the pixel is assigned to cluster C_{j2}. Finally, the splitting of the original cluster is accepted if:

$$\frac{E_j^2}{E_j^1} < 1 - \frac{2}{p\pi} - \alpha\sqrt{\frac{2(1 - \frac{8}{p\pi^2})}{pn_j}}, \tag{10}$$

where $p = 2$ is the dimensionality of the input data set and the constant value α is the upper value corresponding to the 95% percentile of the standard normal distribution [26].

The center and covariance matrix of each nuclei cluster are updated by calculating the mean and covariance matrix of its member pixels, respectively. Then, clusters without any pixel members are deleted and the mean change of the cluster center is estimated since the last iteration are calculated. If the mean change is less than 1 pixel, no more iterations are performed. If these conditions are not met, another iteration is performed, up to a maximum number of iterations that was determined experimentally to be around 10 iterations. The cluster centers at iteration i are retained and the number of pixel members and the covariance matrix of each cluster are both reset to 0, respectively.

The next step consists of hole filling, where connected component analysis is performed on the inverted thresholded image and holes with pixel count greater than $max(n_j)$ are filled up. For connected-component analysis, 4-connectivity is used. This is followed by cell nuclei merging, where we examine the neighbors of each cluster for possible merging. The neighbor clusters are defined as those meeting the following criterion:

$$||\boldsymbol{\mu_i} - \boldsymbol{\mu_j}|| < \alpha(v_i + v_j), \tag{11}$$

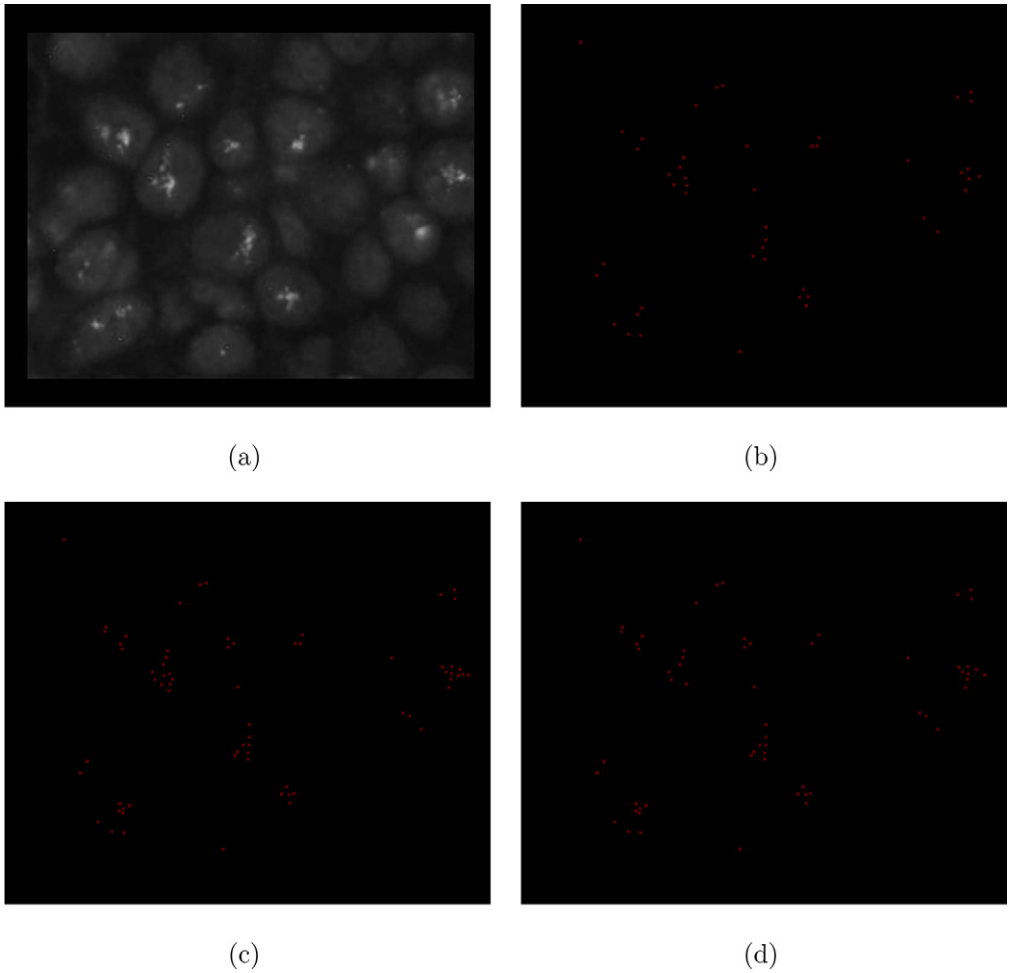

Fig. 5. FISH image spot detection: (a) original red channel, (b) effect of skipping cluster splitting, (c) effect of skipping cluster merging, and (d) final result with cluster splitting and merging. (For interpretation of the references to color in this figure legend, the reader is referred to the web version of the article.)

where $\boldsymbol{\mu_i}$ and $\boldsymbol{\mu_j}$ are the centers and v_i and v_j the principal eigenvalues of clusters C_i and C_j respectively. Next, we calculate the *black pixel fraction* (*BPF*), i.e., the fraction of pixels of the cluster $C_i \bigcup C_j$ that are below a threshold T, i.e., the "black" pixels, as defined by Otsu [22]. The merging of clusters C_i and C_j is decided if:

$$BPF_{i,j} < \beta, \tag{12}$$

where β is the 50% percentile of the exponential distribution, with μ being equal to the mean of the black pixel fraction of all initial nuclei clusters before merging. The exponential distribution was used, because it was experimentally found to fit better the *BPF* distribution across all cell nuclei clusters. The cluster resulting from merging two clusters cannot be merged again during the same iteration. This procedure iterates until no more clusters can be merged. Next, we remove outlier clusters containing too many black pixels that satisfy:

$$BPF_{i,j} > \gamma, \tag{13}$$

where *BPF* is the black pixel fraction, γ is the 95% percentile of the exponential distribution with μ being equal to the mean of the *BPF* of all nuclei after merging. Finally, nuclei clusters touching the image border are also deleted. According to (1), each cell nucleus cluster C_j is spatially modeled by an ellipse, whose region of support can be found by including all pixels $\boldsymbol{X_i}$ satisfying:

$$[\boldsymbol{X_i} - \boldsymbol{\mu_j}]^T \boldsymbol{\Sigma_j}^{-1} [\boldsymbol{X_i} - \boldsymbol{\mu_j}] < \alpha. \tag{14}$$

In Fig. 3, we show the impact of the above described split-merge nuclei segmentation method. More specifically, Fig. 3(a) shows nuclei segmentation of the original FISH image shown in Fig. 1(b), without cluster splitting. We notice that some nuclei are merged together in one cluster. Fig. 3(b) shows the impact of avoiding cluster merging. Nuclei segmentation is observed. Finally, Fig. 3(c) shows the final cell nuclei segmentation by employing all the previously mentioned steps in nuclei segmentation. By combining the information taken from the hole filing procedure with the result from (14) the true cell boundaries can be defined. For a tested FISH image, the resulting images corresponding to the proposed method sub-steps, as shown in Fig. 2, are depicted in Fig. 4.

3.2. Red/green spot detection

Spot detection for the HER-2/neu and CEP 17 probes is performed on the red and green channel separately. Each channel is pre-processed with a succession of steps, commencing with top-hat transform with a disk-shaped structural element of radius 4 [23], followed by thresholding, where the threshold is determined as described in [21]. HER-2/neu and CEP 17 probes appear in both the red and green channels, with HER-2 having higher intensity in the red channel and CEP 17 in the green channel. For this reason, when detecting red spots, we retain only the pixels, whose red channel intensity is at least 10% higher than that of the green channel. For green spot detection we retain only the green channel

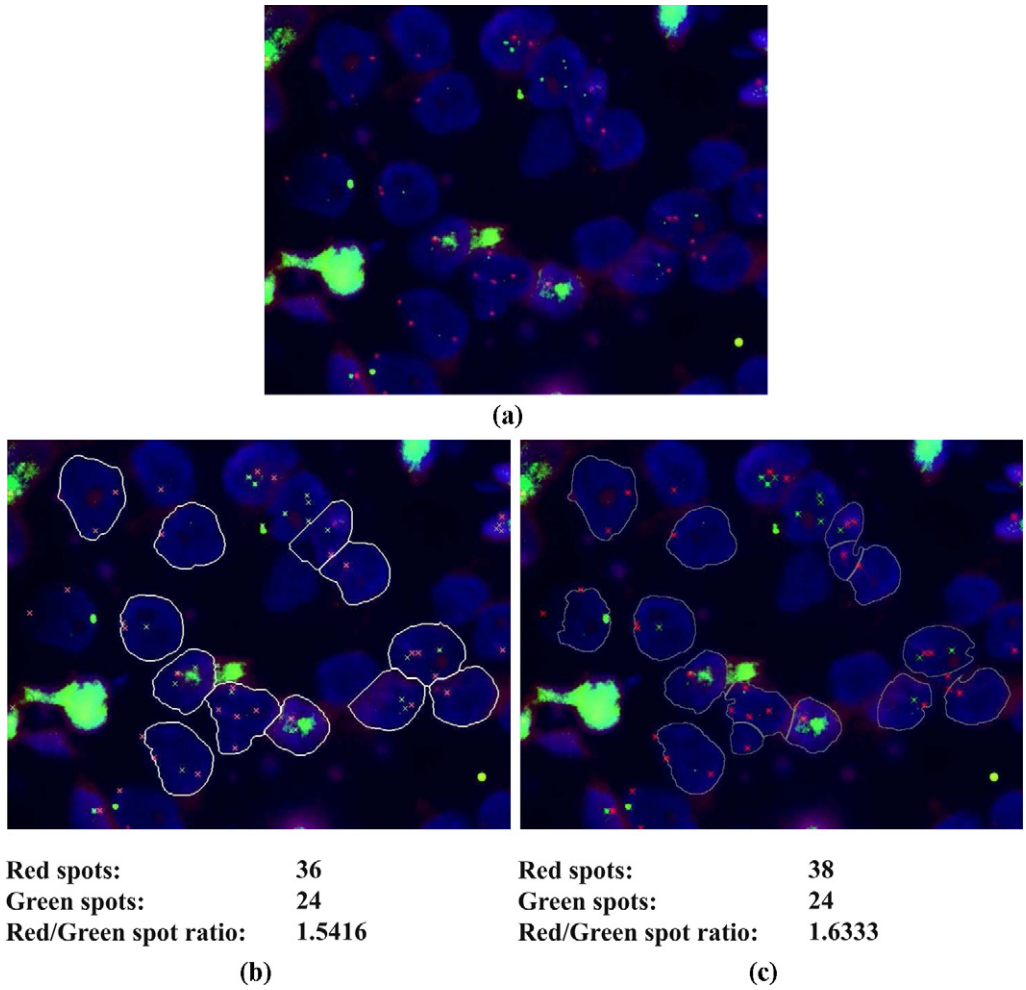

Fig. 6. (a) An example of a tested FISH image and its final cell nuclei segmentation result regarding the abnormal cells based on (b) method [21] and (c) the proposed RBF method.

pixels having intensity at least 10% greater than that of the red channel. The resulting images are called segmented red/green images. The last pre-processing step includes morphological opening with a disk-shaped structural element [23]. Since both red and green spots have circular shape, they can be modeled very well by RBFs of small variance. Therefore, each red or green spot is assumed to be represented by a pixel cluster described by an RBF on the red/green segmented images, respectively. The previously described procedure for cell nuclei segmentation is adapted for red/green spot detection. It is applied on the segmented red/green images independently.

For spot detection in the sub-sampled input images, an adequate large constant number $M = 900$ of initial cluster centers (equal on each segmented red/green image) are initialized at uniform x, y intervals throughout the segmented red/green images, with the cluster covariance matrices initialized to 0. The initial number of cluster centers is deemed to be large enough to cover the vast majority of encountered spot numbers. The segmented red/green image pixels are introduced sequentially to the spot detection algorithm and the corresponding red/green spot clusters are updated according to (5) and (7), while the red/green spot clusters without any members are deleted. After the introduction of each new pixel, red/green spot cluster splitting is considered based on (10). The iteration continues until the mean red/green spot cluster center estimate change is less than 1 pixel or a total number of iterations is reached (it was determined experimentally to be around 10 iterations). Finally, neighbor red/green spot cluster merging is performed if:

$$||\boldsymbol{\mu_i} - \boldsymbol{\mu_j}|| < \zeta max(v_i, v_j), \tag{15}$$

where ζ is the upper value corresponding to the 99% percentile of the standard normal distribution, while v_i and v_j are the principal eigenvalues of clusters i and j, respectively.

Finally, the pixels in a neighborhood around the spot are examined and, if the average intensity of the red channel is not greater than the average intensity of the green channel, when detecting red spots, and vice versa, then the spot is deleted. In addition, spots comprising a very small or very big number of pixels are removed. In Fig. 5, we show the impact of cluster splitting and merging on red spot detection. More specifically, Fig. 5(a) shows the original red channel, while Fig. 5(c and d) shows the resulting red spots, where no splitting, no merging and both splitting and merging are implemented, respectively. It is observed that, without splitting, too few spots are detected, while without merging, some of the detected spots actually correspond to a single spot with slightly larger area. The combination of both splitting and merging enables the more accurate identification of the correct number of red spots. We get similar results for green spot detection.

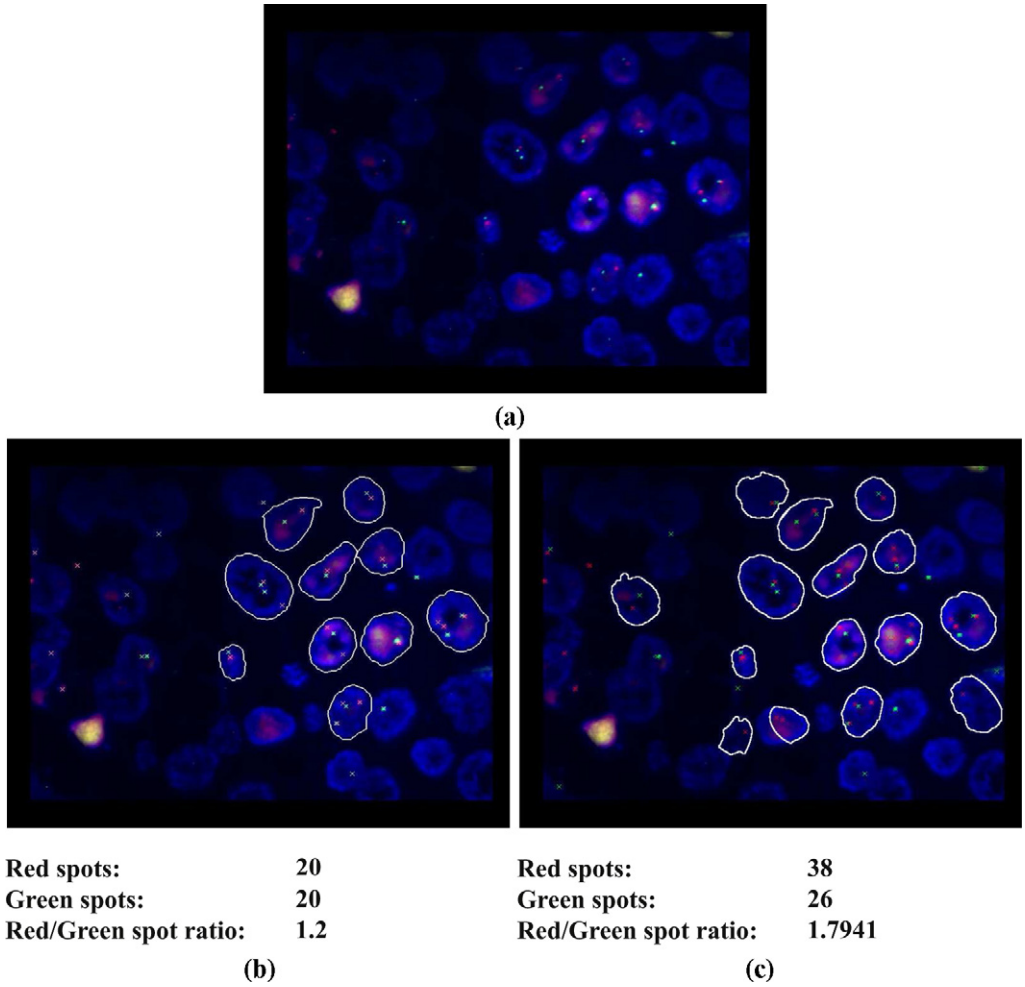

Fig. 7. (a) An example of a tested FISH image and its final cell nuclei segmentation result regarding the abnormal cells based on (b) method [21] and (c) the proposed RBF method.

4. Experimental results in FISH image analysis

As already mentioned, the determination of HER-2/neu gene amplification status involves the calculation of the average red/green spot number ratio in every cell nucleus and the averaging of this ratio over a subset of 'valid' nuclei, i.e. nuclei with at least one red spot. This is typically done over 60 valid nuclei. First we perform cell nuclei segmentation. Then we perform red/green spot detection. In order to calculate the average spot ratio, we use only the ratios corresponding to all valid nuclei. For classification, we classify a breast cancer case as FISH positive or negative, depending on whether the average HER-2/CEP 17 (red/green spot) ratio is greater than or less than 2, respectively.

The FISH image test set provided by the Department Pathology, School of Medicine, Aristotle University of Thessaloniki comprises 246 cases of breast cancer carcinoma. From the total of 246 cases, a subset of 212 ones were classified by the medical experts as negative, while the remaining 34 as positive ones. In total, 3412 FISH images were used in our experiments. Typically, in clinical practice, positive patient cases are far less than the negative ones. Our algorithm was compared to that of [21], which has state of the art performance. Out of the 246 cases analyzed by the algorithm [21], 23 were found positive and 223 negative, while out of 246 cases analyzed by the proposed algorithm, 38 were found positive and 208 negative. Figs. 6 and 7 show the results obtained by method [21] and the proposed RBF method. It is clearly seen that the proposed method out performs that of [21] both in terms of cell nuclei segmentation and red/green spot detection. Table 1 shows the diagnostic accuracy of the two compared algorithms on all the FISH cases, as well as the positive and negative ones. The proposed method had higher overall diagnostic accuracy than that of [21]. In particular, the proposed method had much better overall diagnostic accuracy on the positive FISH cases (91.18% vs. 64.7%). This is extremely important, since the correct identification of positive FISH cases has high impact on the cancer treatment plan. Table 2 shows the red/green spot ratio estimation error, $\boldsymbol{R} = (1/N)\sum_{i=1}^{N} ||r_{d,i} - r_i||$ where $r_{d,i}$, r_i represent the doctor and the algorithmic average spot ratio for case i, respectively. The ratio

Table 1
FISH image classification accuracy.

	Overall accuracy	Accuracy in positive FISH cases	Accuracy in negative FISH cases
Method in [21]	94.72%	64.71%	99.53%
Proposed RBF method	95.93%	91.18%	96.7%

Table 2
Red/green spot ratio estimation error R.

	R for negative FISH cases	R for positive FISH cases
Method in [21]	0.3045	2.22
Proposed RBF method	0.2583	2.16

Table 3
Cohen's Kappa statistical measure and *F*-score as measures of performance of the test [32].

	Positive cases	Negative cases	Number of total cases
Method proposed in [21]			
Positive cases	22	12	34
Negative cases	1	211	212
Number of cases	23	223	246
Results from *F*-score measure			
F = 77.2%, mis-classification rate: 5.3%			
Results from Cohen's Kappa statistical measure			
Kappa = 0.743, 95% confidence interval on Kappa is [0.607, 0.879]			
Proposed RBF method			
Positive cases	31	3	34
Negative cases	7	205	212
Number of cases	38	208	246
Results from *F*-score measure			
F = 86.1%, mis-classification rate: 4.1%			
Results from Cohen's Kappa statistical measure			
Kappa = 0.837, 95% confidence interval on Kappa is [0.739, 0.936]			

estimation error of the proposed algorithm is smaller than that of [21]. Both methods have larger estimation errors in the positive FISH cases than in negative ones, since they cannot count well clotted red spots or defocused red/green spots. However, this is not a major diagnostic problem for the proposed method, since the only diagnostic criterion is whether the red/green spot ratio is above 2. In this respect, the proposed method has very good diagnostic accuracy (91.18%). In general, the proposed RBF technique is faster than the technique proposed in [21]. The execution time for the example depicted in Fig. 6 for method [21] and the proposed RBF method was 6.005 and 4.518 s, while for the example depicted in Fig. 7 the execution time was 8.813 and 3.916 s, respectively.

In order to prove that the improvement of the proposed method is statistically significant, the Cohen's Kappa statistical measure of interrater reliability [31], as well as the *F*-score, which is the weighted harmonic mean of precision and recall, as a single measure of performance of the tests [32] were calculated on the obtained results. Kappa coefficient ranges generally in $[0, \ldots, 1]$ (although negative numbers are possible). Large measure means better reliability. Measure values near or less than zero suggest that improvement is attributable to chance alone. Table 3 shows the results of this statistical measure for both methods, as well as the results from the *F*-score measure. The Kappa coefficient of method [21] is 0.743 and the 95% confidence interval on Kappa lies in the range [0.607, 0.879], while, for the proposed RBF method, Kappa coefficient is 0.837 and the 95% confidence interval on Kappa lies in the range [0.739, 0.936], indicating that the improvement of the proposed method is statistically significant. The *F*-score for the method proposed in [21] is 77.2% with mis-classification rate 5.3%, while, for the proposed RBF method, the *F*-score is 86.1% with mis-classification rate equal to 4.1% indicating that the improvement of the proposed method is statistically significant.

5. Conclusion

We have presented a novel method for analyzing FISH images based on the cell nuclei and spot shape modeling properties of radial basis functions. Our method was compared to a previous method [21] and the comparison showed a significant diagnostic accuracy improvement particularly on HER-2/neu positive cases. The accuracy measurements were performed on a much larger FISH data set than [21]. Furthermore, the experimental results showed that the overall accuracy of the proposed method is very good (95.93%).

Although our method presents a significant improvement vs. the state of art, it is still not perfect and requires supervision by experts, especially at borderline cases, where the ratio is very close to 2. However, a pathologist requires about 30 min to evaluate the HER-2/neu status of a beast carcinoma case, while the proposed method can produce results in less than 5 min. This time is bound to decrease even further, as computer technology advances. It is envisioned that breast carcinoma cases can be initially screened by our algorithm. A second screening by a pathologist was measured to require only 5 min, since the doctor typically only surveys the results of the automated algorithm and makes some minor changes to nuclei segmentation and/or spot counting. This combined semi-automatic approach involving doctor supervision results to an increase in overall FISH diagnosis speed by a factor of at least three. As a conclusion, the presented method shows great promise in aiding routine FISH diagnosis for numerous breast carcinoma patients.

References

[1] P.P. Osin, S.R. Lakhani, The pathology of familial breast cancer: immunohistochemistry and molecular analysis, Breast Cancer Research 1 (1) (1999) 36–40.
[2] J.S. Ross, J.A. Fletcher, K.J. Bloom, G.P. Linette, J. Stec, W.F. Symmans, et al., Targeted therapy in breast cancer: the her-2/neu gene and protein, Molecular and Cellular Proteomics 3 (4) (2004) 379–398.
[3] O.P. Kalliomeni, A. Kalliomeni, W. Kurisu, A. Thor, L.C. Chen, H.S. Smith, et al., Erbb2 amplification in breast cancer analyzed by fluorescence in situ hybridization, Proceedings of the National Academy of Sciences of the United States of America 89 (12) (1992) 5321–5325.
[4] D.N. Shapiro, M.B. Valentine, S.T. Rowe, A.E. Sinclair, J.E. Sublett, W.M. Roberts, et al., Detection of n-myc gene amplification by fluorescence in situ hybridization. Diagnostic utility for neuroblastoma, Journal of Pathology 142 (5) (1993) 1339–1346.
[5] J. Bartlett, E. Mallon, T. Cooke, The clinical evaluation of her-2 status: which test to use? Journal of Pathology 199 (4) (2003) 411–417.
[6] J. Klijanienko, J. Couturier, M. Galut, A.K. El-Naggar, Z. Maciorowski, E. Padoy, et al., Detection and quantification by fluorescence in situ hybridization (fish) and image analysis of her-2/neu gene amplification in breast cancer fine-needle samples, Cancer Cytopathology 87 (5) (1999) 312–318.
[7] J.L. Fernandez, V. Goyanes, C.L. Fernandez, I. Buno, J. Gosalvez, Quantification of c-erb-b2, gene amplification in breast cancer cells using fluorescence in situ hybridization and digital image analysis, Cancer Genetics and Cytogenetics 86 (1) (1996) 18–21.
[8] H. Netten, I.T. Young, L.J. van Vliet, H.J. Tanke, H. Vroljik, W.C.R. Sloos, Fish and chips: automation of fluorescent dot counting in interphase cell nuclei, Cytometry 28 (1) (1997) 1–10.
[9] H. Netten, L.J. van Vliet, H. Vroljik, W.C.R. Sloos, H.J. Tanke, I.T. Young, Fluorescent dot counting in interphase cell nuclei, Bioimaging 4 (1996) 93–106.
[10] T.W. Ridler, S. Calvard, Picture thresholding using an iterative selection method, IEEE Transactions on Systems, Man, and Cybernetics SMC-8 (8) (1978) 630–632.
[11] C.O. de Solorzano, A. Santos, I. Vallcorba, J.M. Garcia-Sagredo, F. del Pozo, Automated fish spot counting in interphase nuclei: statistical validation and data correction, Cytometry 31 (2) (1998) 93–99.
[12] L. Vincent, Morphological grayscale reconstruction in image analysis: applications and efficient algorithms, IEEE Transactions on Image Processing 2 (2) (1993) 176–201.
[13] M. Kozubek, S. Kozubek, E. Lukasova, A. Mareckova, E. Bartova, M. Skalnikova, et al., High-resolution cytometry of fish dots in interphase nucleus nuclei, Cytometry 36 (4) (1999) 279–293.
[14] W.K. Pratt, Digital Image Processing, John Wiley & Sons Inc., New York, 1991.
[15] B. Lerner, W.F. Clocksin, S. Dhanjal, M.A. Hulten, C.M. Bishop, Feature representation and signal classification in fluorescence in-situ hybridization image analysis, IEEE Transactions on Systems, Man, and Cybernetics 31 (6) (2001) 655–665.
[16] W.F. Clocksin, B. Lerner, Automatic analysis of fluorescence in-situ hybridization images, in: Proceedings of the 11th British Machine Vision Conference, September, vol. 89 (12), 2000, pp. 666–674.
[17] M.K. Chawla, G. Lin, K. Olson, A. Vazdarjanova, S.N. Burke, B.L. McNaughton, et al., 3d-catfish: a system for automated quantitative three-dimensional compartmental analysis of temporal gene transcription activity imaged by fluorescence in situ hybridization, Journal of Neuroscience Methods 139 (2004) 13–24.
[18] J.N. O'Sullivan, J.C. Finley, R.A. Risques, W. Shen, K.A. Gollahon, A.H. Moskovitz, et al., Telomere length assessment in tissue sections by quantitative fish: image analysis algorithms, Cytometry 58 (2) (2004) 120–131.
[19] H. Masmoudi, S. Hewitt, N. Petrick, K. Myers, M. Gavrielides, Automated quantitative assessment of her-2/neu immunohistochemical expression in breast cancer, IEEE Transactions on Medical Imaging 28 (6) (2009) 916–925.

[20] B. Reljin, M. Paskas, I. Reljin, K. Konstanty, Breast cancer evaluation by fluorescent dot detection using combined mathematical morphology and multifractal techniques, in: Proceedings of the 10th European Congress on Telepathology and 4th International Congress on Virtual Microscopy Vilnius, 1–3 July, vol. 6 (S21), 2010.
[21] F. Raimondo, M.A. Gavrielides, G. Karayannopoulou, K. Lyroudia, I. Pitas, I. Kostopoulos, Automated evaluation of her-2/neu status in breast tissue from fluorescent in situ hybridization images, IEEE Transactions on Image Processing 14 (9) (2005) 1288–1299.
[22] N. Otsu, A thresholding selection method from graylevel histogram, IEEE Transactions on Systems, Man and Cybernetics 9 (1) (1979) 62–66.
[23] I. Pitas, Nonlinear Digital Filters: Principles and Applications, Kluwer Academic, 1990.
[24] M.D. Buhmann, Radial Basis Functions: Theory and Implementations, Cambridge University Press, 2003.
[25] A. Papoulis, Probability, Random Variables and Stochastic Processes, McCraw-Hill, New York, 1984.
[26] C. Kotropoulos, I. Pitas, A variant of learning vector quantizer based on split-merge statistical tests, Lecture Notes in Computer Science: Computer Analysis of Images and Patterns 7 (19) (1993) 822–829.
[27] J.A. Kangas, T.K. Kohonen, J.T. Laaksonen, Variants of selforganizing maps, IEEE Transactions Neural Networks 1 (1990) 93–99.
[28] E. Yair, K. Zeger, A. Gersho, Competitive learning and soft competition for vector quantizer design, IEEE Transactions Signal Processing 40 (2) (1992) 294–309.
[29] S. Chen, B. Mulgrew, Overcoming cochannel interference using an adaptive radial basis functions equalizer, Signal Processing 28 (1992) 91–107.
[30] S. Chen, B. Mulgrew, P.M. Grant, A clustering technique for digital communications channel equalization using radial basis function networks, IEEE Transactions Neural Networks 4 (1993) 570–579.
[31] J.R. Landis, G.G. Koch, The measurement of observer agreement for categorical data, Biometrics 33 (1977) 159–174.
[32] G.W. Snedecor, W.G. Cochran, Statistical Methods, eighth ed., Iowa State University Press, 1989.